JSR Publications

Available Online

J. Sci. Res. **18** (1), 67-79 (2026)

JOURNAL OF SCIENTIFIC RESEARCH

www.banglajol.info/index.php/JSR

Comprehensive Characterization and Nonlinear Optical Properties of L-Histidine Diglycine Picrate (LHSDGP) Single Crystals for Advanced Photonic Applications

R. Suganthi*, K. Balasubramanian

PG & Research Department of Physics, The M.D.T. Hindu college, Affiliated to Manonmaniam Sundaranar University, Abishekapatti – 627012, Tirunelveli, Tamil Nadu, India

Received 26 April 2025, accepted in final revised form 28 October 2025

Abstract

The L-Histidine Diglycine Picrate (LHSDGP) single crystal was carefully synthesized at room temperature using the slow evaporation solution technique (SEST), which allows for the gradual formation of LHSDGP crystals from a supersaturated solution under controlled conditions. The crystal's structure was confirmed through Single Crystal X-ray Diffraction, revealing an orthorhombic lattice within the $P2_12_12_1$ space group. To further validate its structural consistency, Powder X-ray Diffraction studies were also conducted. Fourier Transform Infrared (FTIR) spectroscopy was used for vibrational analysis, aiding in the identification of molecular groups and providing insight into the crystal's chemical composition. The mechanical properties of the crystal were assessed using microhardness testing, demonstrating its durability. Optical properties, including light absorption and transmission characteristics, were examined through UV-vis-NIR spectroscopy. The LHSDGP crystal's electrical response was analyzed through dielectric measurements, tracking changes in the dielectric constant and loss factor at three different temperatures. The TG/DTA analysis was conducted to determine the decomposition temperature and thermal endurance of the LHSDGP crystal. Notably, the laser damage threshold (LDT) of LHSDGP was found to be 2.7 GW/cm², highlighting its potential for high-power laser applications. Z-scan techniques evaluated the LHSDGP crystal's third-order nonlinear optical properties.

Keywords: Structural analysis; Optical properties; Electrical properties; Thermal stability; Laser resistance; Nonlinear optics.

doi: https://dx.doi.org/10.3329/jsr.v18i1.81278 J. Sci. Res. **18** (1), 67-79 (2026)

1. Introduction

Organic crystals, formed through the ordered assembly of molecules, have emerged as vital materials in nonlinear optics due to their remarkable ability to manipulate light. These crystals are extensively utilized in photonic and optoelectronic devices such as harmonic generators, optical switches, and frequency converters [1-5]. Their molecular tunability allows for precise control over optical responses, enabling applications across

* *Corresponding author*: jerusharma2014@gmail.com

communication technologies, biomedical imaging, and photonic signal processing. Amino acid-based crystals have recently gained attention for enhancing nonlinear optical effects. L-Histidine, in particular, is notable for its imidazole group that promotes effective charge transfer, resulting in pronounced second- and third-order nonlinearities [6-8]. Furthermore, its inherent biocompatibility and environmental resilience make it appealing for biomedical and sensing uses. On the other hand, Diglycine Picrate (DGP) is well-known for its strong third-order nonlinear optical properties, including optical limiting and self-focusing, combined with excellent thermal and mechanical stability and a high laser damage threshold [9]. Despite the individual merits of L-Histidine and DGP, research exploring their combination in a single crystalline system remains scarce. The integration of these components could unlock synergistic effects, potentially enhancing third-order nonlinear optical performance for advanced photonic applications [10-12]. This study focuses on the synthesis and thorough characterization of a novel L-Histidine Diglycine Picrate (LHSDGP) crystal. Comprehensive analyses, including X-ray diffraction (XRD), Fourier-transform infrared spectroscopy (FTIR), UV-Vis-NIR spectroscopy, microhardness testing, dielectric measurements, thermogravimetric and differential thermal analysis (TG-DTA), and laser damage threshold (LDT) assessment, were conducted. Third-order nonlinear optical parameters were evaluated using the Z-scan technique, demonstrating the LHSDGP crystal's promising potential for nonlinear photonics.

2. Experimental Details

2.1. *Growth and synthesis procedure*

The LHSDGP compound was synthesized using the slow evaporation solution technique. L-Histidine and Diglycine picrate were mixed in distilled water in a 1:1 ratio. Each substance was initially dissolved separately, then the solutions were combined and stirred for 8 hours to ensure complete reaction. The resulting yellow solution was left to evaporate slowly at ambient temperature, leading to the formation of yellow LHSDGP crystals. After 14 days, a well-formed single crystal of LHSDGP, measuring 8×6×3 mm^3, had grown. Fig. 1 shows an image of the LHSDGP single crystal.

Fig. 1. As grown LHSDGP single crystal.

2.2. *Characterization techniques*

A comprehensive characterization of the LHSDGP crystal was carried out using various advanced techniques across institutions in India. Single crystal X-ray diffraction was performed using a BRUKER AXS (Kappa APEXII) diffractometer with MoKα radiation (λ = 0.71073 Å) at SAIF, IIT Chennai, India, and powder XRD was done using a BRUKER D8 ADVANCE at the Materials Research Centre, Saveetha Dental College, Chennai, India. FTIR spectroscopy (400-4000 cm^{-1}) was conducted using a BRUKER AXS instrument at the same facility. Mechanical properties were studied using a SHIMADZU HMV-G21 Vickers microhardness tester at St. Joseph's College, Tiruchirappalli, India. Optical behavior was analyzed using a JASCO V-730 UV-Vis spectrophotometer at Saveetha Dental College, India. Dielectric measurements were performed using an Agilent E4980A LCR meter (50 Hz-2 MHz) at St. John's College, Palayamkottai, India. Thermal stability was assessed with a Perkin-Elmer Diamond TG/DTA instrument at Noorul Islam Centre for Higher Education, Kanyakumari, India. Laser damage threshold was measured using a Q-switched Nd:YAG laser (1064 nm, QUANTA RAY) at B.S. Abdur Rahman Crescent Institute of Science and Technology, Chennai, India. Finally, third-order nonlinear optical susceptibility was investigated via Z-scan using a continuous wave laser (21 mW, 632.8 nm) at SSN Research Centre, SSN College of Engineering, Chennai, India.

3. Results and Discussion

3.1. *Structural analysis through XRD evaluation*

Single crystal XRD shows how atoms are arranged in a crystal. It gives exact details about atom positions, bond lengths, and angles [13-15]. The lattice parameters for LHSDGP are given as follows: a = 6.87Å, b = 8.92Å, c = 15.30Å, with α = 90°, β =90°, and γ = 90°. The calculated volume is V = 938$Å^3$. The measurements show that the LHSDGP crystal belongs to the orthorhombic crystal system and is assigned to the centrosymmetric space group $P2_12_12_1$. The single crystal XRD data for both DGP and LHSDGP crystals are presented in Table 1. Powder XRD analyzes the crystal structure of powders. It identifies phases, crystal size, and structural details [16,17]. The LHSDGP measurements were performed over a 2θ range of 10 to 70 degrees at room temperature. The analysis of the resulting graph revealed a peak intensity at 24.126°, demonstrating the superior crystalline quality of the LHSDGP crystal, with sharp, high-intensity peaks. Fig. 2 shows the PXRD spectra of LHSDGP, and detailed powder XRD data for LHSDGP are provided in Table 2.

Table 1. SXRD results for LHSDGP crystal.

Crystal Name	Lattice parameters	Volume $(Å)^3$	Z	Crystal System	Space group
Diglycine Picrate (DGP)	a = 15.142Å b = 6.654 Å c = 15.367 Å α = 90^0; β=93^0 γ = 90^0	1541.47	2	Monoclinic	Centrosymmetric $P2_1/C$

L-Hisditine Diglycine Picrate (LHSDGP)	a = 6.87Å b = 8.92 Å c = 15.30 Å $\alpha = 90^0$; $\beta = 90^0$ $\gamma = 90^0$	938	4	Orthorhombic P	Centrosymmetric $P2_12_12_1$

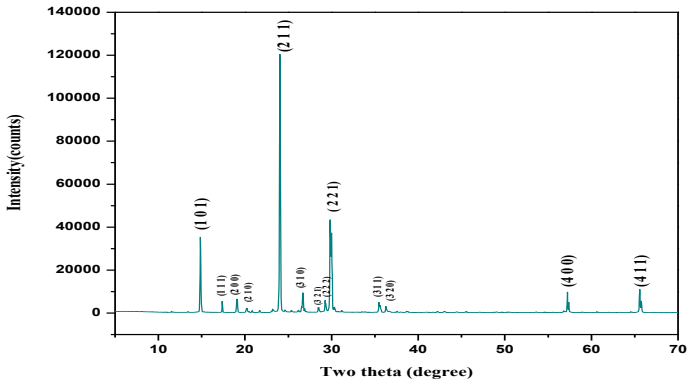

Fig. 2. XRD Pattern of LHSDGP with hkl Indices

Table 2. PXRD information for LHSDGP crystal.

Pos.[◦2Th.]	Height[cts]	d spacing[Å]	FWHM[◦2Th.]	Rel.int.[%]	hkl
14.903	22194.2	5.93964	0.104	56.6	1 0 1
17.398	4346.74	5.09317	0.085	11.1	1 1 1
19.061	5736.82	4.65236	0.148	14.6	2 0 0
20.270	1335.87	4.37740	0.162	3.4	2 1 0
24.126	39206.0	3.68589	0.125	100	2 1 1
26.772	2855.29	3.32731	0.115	7.3	3 1 0
28.586	1070.57	3.12013	0.159	2.7	3 2 1
29.342	3338.31	3.04144	0.137	8.5	2 2 2
29.871	34422.4	2.98875	0.266	87.8	2 2 1
35.465	4555.91	2.52909	0.211	11.6	3 1 1
36.297	2028.24	2.47303	0.097	5.2	3 2 0
57.161	2004.49	1.61017	0.072	5.1	4 0 0
65.477	1373.93	1.42436	0.107	3.5	4 1 1

3.2. *Analysis using FTIR spectroscopy*

FTIR analysis shines infrared light on crystals to study their bond vibrations. This produces a unique pattern that helps identify the crystal's chemicals. It's useful for both organic and inorganic crystals [18-20]. Fig. 3 shows the FTIR spectrum of LHSDGP, recorded using the KBr pellet method in the 1000-4000 cm^{-1} range. The spectrum exhibits broad features between 1600-2900 cm^{-1}. The O-H stretching for alcohols appears at 3153.12 cm^{-1} with a weak intensity, while for carboxylic acids, the O-H stretching occurs at 2612.61 cm^{-1} and is strong. The N-H stretching of amine salts is observed at 2820.61 cm^{-1}, showing a strong

absorption [21]. A C = O stretching at 1579.33 cm^{-1} corresponds to unhydride groups and has a strong intensity. Nitro compounds exhibit an N-O stretching at 1497.58 cm^{-1}, also with a strong intensity. Sulfates show an S=O stretching at 1405.54 cm^{-1}, which is strong, as is the S=O stretching for sulfoxides at 1032.34 cm^{-1}. Alcohols also exhibit O-H bending at 1330.19 cm^{-1}, with medium intensity. For amines, the C-N stretching at 1109.43 cm^{-1} is categorized as medium. Alkenes show C = C bending at 908.04 cm^{-1}, while disubstituted alkenes show a similar C = C bending at 891.14 cm^{-1}, both with strong intensity. Finally, a strong C-I stretching at 692.94 cm^{-1} characterizes the halo compound class. These vibrational assignments provide insights into the functional groups present in the L-histidine diglycine picrate(LHSDGP) crystal and their characteristic IR absorption features.

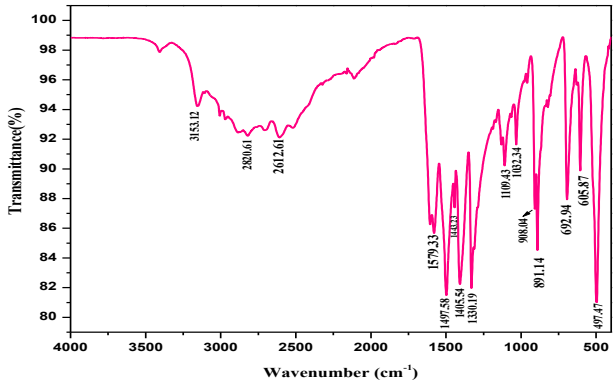

Fig. 3. FTIR spectrum for LHSDG.

3.3. *Microhardness analysis*

Microhardness analysis tests the hardness of small crystal spots by pressing a sharp indenter into the surface with a set force. The size of the indentation shows how hard the material is. This helps assess mechanical strength for applications like microelectronics and coatings [22-24]. Smaller indentations indicate harder materials. The hardness value is calculated using the following equation,

$$H_v = 1.8544\ P/d^2\ kg/mm^2$$

where 'H_v' is the hardness value, 'P'is the applied load in kilograms, and 'd' signifies the mean diagonal measurement of the indentation in millimeters. Fig. 4a presents a plot of the logarithms of the applied load (P) and the diagonal length (d). From this, a measured value of n (B = 0.26145) is observed, categorizing the LHSDGP crystal as a hard material. Fig. 4b illustrates the relationship between the hardness value (H_v) and the applied load (P), showing that as the load increases from 25 g to 100 g, the hardness value rises in a linear fashion. The hardness data for the LHSDGP crystal indicates that it requires a greater amount of stress to induce micro-damage, suggesting its high crystalline quality [25]. This feature makes the LHSDGP crystal particularly well-suited for device fabrication.

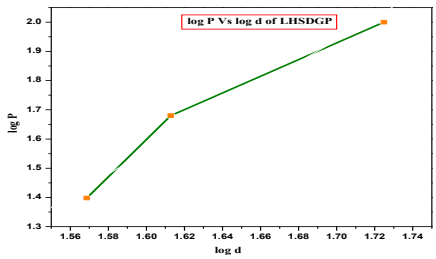

Fig. 4a. log P vs log d of LHSDGP.

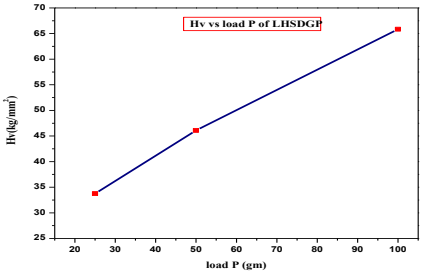

Fig. 4b. H_v vs load P of LHSDGP.

3.4. *UV-Vis-NIR analysis*

The ltraviolet (UV) studies on crystals are used to investigate their optical properties and electronic structures by observing how they absorb, reflect, or transmit UV light. These interactions provide valuable insights into the material's bandgap, defects, and electronic behavior [26]. Techniques like UV-visible spectroscopy are commonly employed to examine these characteristics. The optical characteristics of the LHSDGP single crystal are comprehensively illustrated in Fig. 5a. The title crystal demonstrates an impressive transmittance rate of 95 % across a broad wavelength range from 500 to 800 nm, showcasing its potential for a variety of optical applications [27]. The crystal's high transparency in the UV-visible near-infrared spectrum, with minimal absorption, is particularly noteworthy. Fig. 5b highlights the energy band gap of LHSDGP, with an optical band gap of 2.7 eV determined from the linear segment of the αhν vs hν plot. Fig. 5c presents the absorption spectrum, revealing distinct absorption peaks at 245 and 350 nm, corresponding to $\pi \rightarrow \pi^*$ and $n \rightarrow \pi^*$ transitions within the LHSDGP crystal. Fig. 5d illustrates the increase in optical conductivity in the visible region at a wavelength of 370 nm, emphasizing the crystal's potential for optoelectronic device design. Fig. 5e shows the variations in the refractive index with wavelength, where LHSDGP exhibits a notably low refractive index of 0.01680 in the visible spectrum, which decreases as the wavelength increases [28]. Finally, Fig. 5f demonstrates the extinction coefficient's behavior with wavelength, showing a minimum in the visible range, indicating minimal absorption of radiation [29]. In conclusion, the LHSDGP crystal's broad band gap, low refractive index in the visible range, and wide transmission range make it a promising candidate for advanced optoelectronic applications.

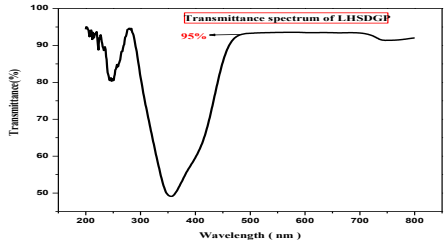

Fig. 5a. Transmission versus wavelength.

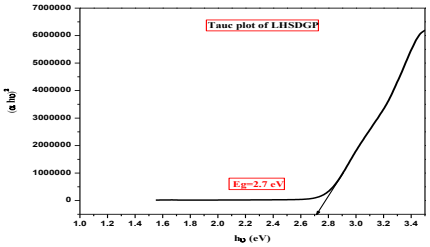

Fig. 5b. Tauc plot of LHSDGP.

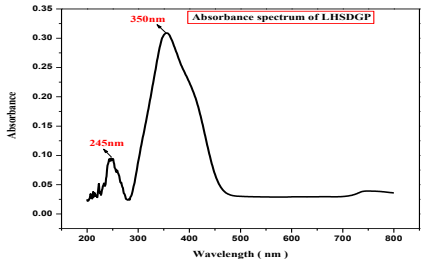

Fig. 5c. Absorbance versus wavelength.

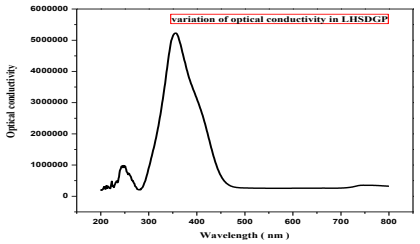

Fig. 5d. Optical conductivity of LHSDGP.

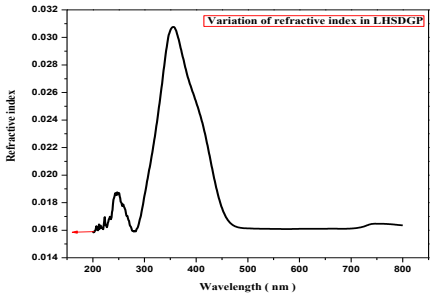

Fig. 5e. Refractive index versus wavelength.

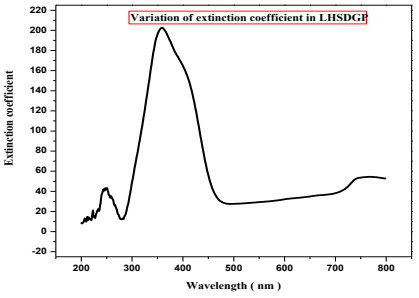

Fig. 5f. Extinction coefficient of LHSDGP.

3.5. *Thermal analysis*

TG/DTA analyzes crystals by tracking weight and heat flow changes during heating or cooling. It helps detect phase transitions, melting, dehydration, and decomposition, giving insight into stability and purity [30-32]. In this study, a 1.50 mg sample was subjected to thermal analysis over a temperature range of 100 to 800 °C, with a heating rate of 20 °C per minute in a nitrogen atmosphere. The TG analysis revealed that the LHSDGP crystal remains stable up to 150 °C, after which it begins to lose weight, with complete decomposition occurring at 280 °C. The DTA analysis identified the melting point of the LHSDGP crystal at 270 °C, indicated by a clear endothermic peak, which emphasizes the

high crystalline quality of the LHSDGP crystal [33,34]. The TG-DTA spectrum of the LHSDGP single crystal is shown in Fig. 6.

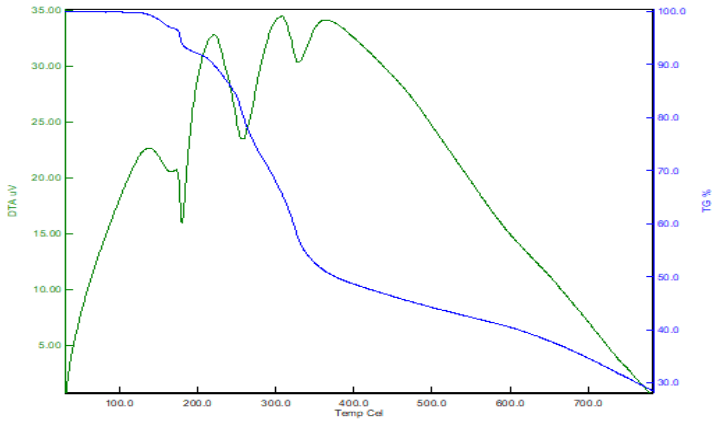

Fig. 6. TG/DTA curves of LHSDGP

3.6. *Dielectric study*

Dielectric studies explore electrical properties of crystals, such as permittivity and dielectric constant.These properties depend on the crystal structure and reveal charge transport and polarization behavior.Such insights are essential for improving devices like capacitors, sensors, and other electronics[35-37]. Dielectric analysis of LHSDGP single crystals evaluated their permittivity and loss over a frequency range of 1 Hertz to 1 Mega Hertz at temperatures of 30 °C, 50 °C, and 70 °C. Figs. 7a-b depict the relationship between dielectric constant and loss. In Fig. 7a, a distinct increase in dielectric constant is observed within a narrow frequency range at all tested temperatures, indicating the involvement of multiple polarization mechanisms, including ionic, electronic, space charge, and orientation [38]. At high frequencies, the dielectric constant drops due to reduced space charge polarization at grain boundaries. Materials with high dielectric constants at low frequencies are ideal for energy storage, efficient capacitors, and electromagnetic shielding because they store more charge. Fig. 7b shows that LHSDGP crystals display low dielectric loss (tan δ) at all temperatures, reflecting their high optical quality and minimal defects, making them suitable for nonlinear optics (NLO) applications. Low dielectric loss improves optical communication by enabling faster data transfer with minimal signal degradation over long distances [39]. Fig. 7c illustrates that AC conductivity in LHSDGP crystals increases with frequency, which can significantly boost the performance of nonlinear optical devices. Table 4 provides activation energy values for LHSDGP, offering additional insights into its electrical properties under various conditions.

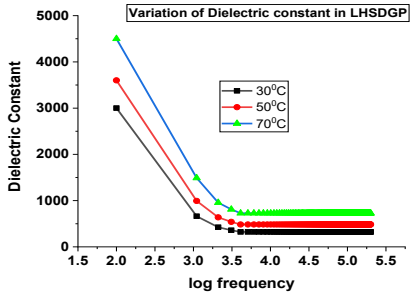

Fig. 7a. Dielectric constant in LHSDGP.

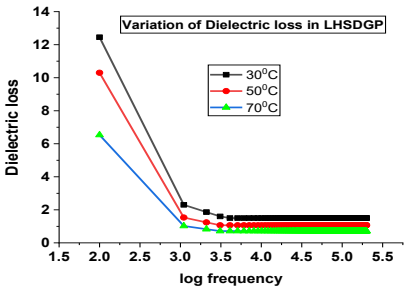

Fig. 7b. dielectric loss in LHSDGP.

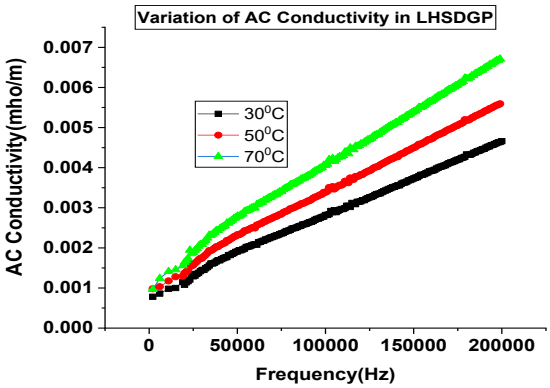

Fig. 7c. AC conductivity in LHSDGP.

Table 4. Activation energy in LHSDGP.

Frequency(Hz)	Ea/K	Ea(LHSDGP)
100	0.4234	3.64844E-05
1099	0.3245	2.79622E-05
10095	0.2956	2.54719E-05
50075	0.1345	1.15899E-05
100050	0.1238	1.06678E-05
200000	0.0896	7.72083E-06

3.7. *Laser Damaged Threshold (LDT) study*

The LDT tests measure the highest laser intensity a crystal can handle without damage. This helps assess the crystal's durability for high-power laser uses, like laser sources and optical coatings. Knowing the LDT helps choose materials that work reliably in intense laser environments [40-42]. Such studies are essential for optimizing crystal materials for use in laser systems, ensuring both efficiency and longevity. The investigation of the laser damage threshold involved subjecting LHSDGP crystals to high-intensity radiation from a Q-switched (Nd-YAG) laser operating at 1064 nanometers. The laser emitted pulses with a

duration of 6 nanoseconds at a frequency of 10 Hertz, which were focused onto the LHSDGP crystal using a lens with a 10 cm focal length. The pulse energy was precisely measured using a power meter, and the energy density was calculated using the following formula,

Power density, $P_d = \frac{E}{\tau \pi r^2}$.

In this equation, 'E' stands for the energy density input measured in millijoules (mJ), 'τ' represents the pulse duration in nanoseconds (ns), and 'r' indicates the radius of the laser spot in millimeters (mm). The LHSDGP crystal exhibited an impressive laser damage threshold of 1.1 gigawatts per square centimeter (GW/cm²), significantly surpassing the thresholds of conventional materials such as KDP (0.20 GW/cm²) and urea (1.50 GW/cm²), though slightly lower than the urea value The LHSDGP crystal's strong resistance to laser damage highlights its potential in advanced technologies. It's suitable for high-power lasers, optical communication, and fusion energy research [43].These applications require optical components that can withstand extreme laser conditions, offering significant improvements in efficiency and performance [44].

3.8. *Z-Scan investigation*

Z-scan analysis is a useful technique to study the nonlinear optical properties of materials like crystals. It measures how a laser beam's transmission changes as the crystal moves along the beam's path. This helps determine important properties like nonlinear absorption, refraction, and third-order susceptibility [45-48]. In this experiment, a polarized Gaussian beam in TEM00 mode was focused using a 300 mm focal length lens, resulting in a beam waist of ω_0 = 16.1 μm for the LHSDGP crystal. The crystal's thickness was 1 mm, and the Rayleigh length (ZR) was 1.3 mm, ensuring that the crystal thickness (L) was smaller than the ZR, which is important for proper measurement. The sample holder was moved using a computer-controlled motor, while a digital power meter recorded the transmitted intensity. In the closed-aperture setup with a 2 mm aperture, a peak-to-valley variation was observed, indicating a self-defocusing effect, as shown in Fig. 8a. In the open-aperture setup, the lowest transmittance occurred at the focal point, demonstrating reverse saturable absorption, as illustrated in Fig. 8b, confirming that the nonlinear absorption coefficient (β) is positive [49,50]. The LHSDGP crystal exhibits significant nonlinear optical properties, including a negative nonlinear refractive index of $-.8590\times10^{-12}$ m²/W, a positive nonlinear absorption coefficient of 1.2618×10^{-7} m/W, and a high third-order nonlinear susceptibility of 4.8441×10^{-10} esu. The LHSDGP crystal's negative nonlinear refractive index causes self-defocusing, aiding optical switching and pulse shaping [51-53]. Its positive nonlinear absorption causes reverse saturable absorption, protecting devices from strong laser pulses. Its high third-order susceptibility supports frequency conversion and signal processing, making it useful for advanced optical technologies [54].

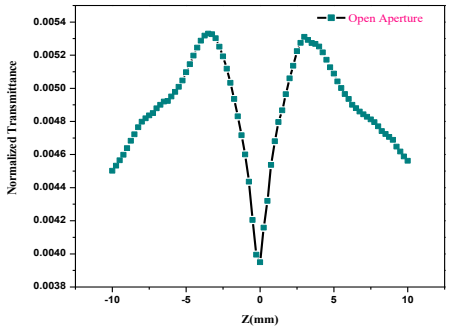

Fig. 8(a). Open aperture spectrum of LPADGP.

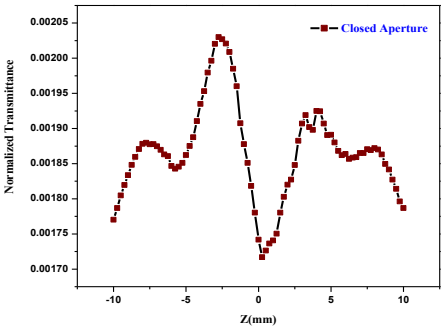

Fig. 8(b). Closed aperture spectrum of LHSDGP.

4. Conclusion

A high-quality LHSDGP organic crystal was successfully synthesized using the slow evaporation solution method, resulting in a transparent yellow crystal with dimensions of 8×6×3 mm³. Single crystal XRD analysis confirmed the orthorhombic P212121 structure within the centrosymmetric space group. Powder X-ray diffraction further validated the crystal's high purity, while FTIR spectroscopy provided insights into its functional groups and vibrational modes. The crystal's mechanical strength was evaluated using Vickers microhardness testing, and UV-Vis-NIR spectroscopy demonstrated outstanding optical transparency of 95 %, with absorption cut-off wavelengths at 245 nm and 350 nm, making it ideal for NLO applications. Dielectric loss measurements at elevated frequencies (30 °C, 50 °C, and 70 °C) revealed minimal losses, while the crystal exhibited a laser damage threshold of 1.1 GW/cm², highlighting its durability for laser-based applications. Thermal analysis, through TG and DTA, showed that the crystal retains its structural integrity up to 150 °C. Additionally, the high third-order susceptibility value (χ^3 = 4.8441×10^{-10} esu) further bolsters its potential for all-optical switching, nonlinear frequency conversion, and photonic signal processing.

References

1. S. Sivaraman, C. Balakrishnan, A. A. Prasad, R. M. Sokalingam, S. P. Meenakshisundaram, and R. Markkandan, Mol. Cryst. Liq. Cryst. **656**, 153 (2017). https://doi.org/10.1080/15421406.2017.1401291
2. S. R. Thilagavathy and K. Ambujam, Trans. Indian Inst. Met. **64**, 143 (2011). https://doi.org/10.1007/s12666-011-0028-2
3. V. V. Ghazaryan, M. Fleck, and A. M. Petrosyan, Spectrochim. Acta A. Mol. Biomol. Spectrosc. **78**, 128 (2011). https://doi.org/10.1016/j.saa.2010.09.009
4. N. Balasundari, P. Selvarajan, S. L. M. Ponmani, and D. Jencylin, Recent Res. Sci. Technol. **3**, 12 (2012).

5. B. R. Srinivasan, N. U. Parsekar, R. A. Apreyan, and A. M. Petrosyan, Mol. Cryst. Liq. Cryst. **680**, 75 (2019). https://doi.org/10.1080/15421406.2019.1624027
6. P. Sangeetha, P. Jayaprakash, P. R amesh, S. Sudha, G. Vinitha, M. Nageshwari, and M. L. Caroline, J. Mol. Struct. **1213**, ID 128187 (2020). https://doi.org/10.1016/j.molstruc.2020.128187
7. S. Guha, Indian J. Phys. **44**, 267 (1970). https://doi.org/10.2307/40124349
8. J. J. Madden, E. L. McGandy, N. C. Seeman, M. M. Harding, and A. Hoy, Struct. Sci. **28**, 2382 (1972). https://doi.org/10.1107/S056774087200617X
9. S. Sagadevan and R.Varatharajan, Mat. Phys. Mech. **18**, 11 (2013).
10. H. Fuess, D. Hohlwein, and S. A. Mason, Struct. Sci. **33**, 654 (1977). https://doi.org/10.1107/S0567740877004415
11. V. Kannan, R. B. Ganesh, and P. Ramasamy, Cryst. Growth Des. **6**, 1876 (2006). https://doi.org/10.1021/cg0601960
12. J. J. Madden, E. L. McGandy, and N. C. Seeman, Struct. Sci. **28**, 2377 (1972). https://doi.org/10.1107/S0567740872006168
13. J. Priscilla, G. V. Vijayaraghavan, and K. Y. Kumar, J. Mat. Sci. Mat. Electron. **35**, 1265 (2024). https://doi.org/10.1007/s10854-024-13070-w
14. D. R. Manley, M.Sc. thesis, Polytechnic Institute of Brooklyn, USA, 1936.
15. B. S. Kumar and K. R. Babu, Indian J. Pure Appl. Phys. **46**, 123 (2008).
16. S. Suresh and M.Vijayan, Struct. Sci. **52**, 876 (1996). https://doi.org/10.1107/S0108768196005368
17. P. R. Deepthi and J. Shanthi, Int. J. **2**, 815 (2014).
18. A. Alexandar, I. Johnson, A. M. Dayana,T. S. Girisun, B. S. I. Lasalle, and M. S. Pandian, Inorg. Chem. Commun. **159**, ID 111751 (2024). https://doi.org/10.1016/j.inoche.2023.111751
19. E. Shobhana, B. Balraj, B. Mohanbabu, and V. Sathyanarayanamoorthi, Asian J. Chem. **35**, 2603 (2023). https://doi.org/10.14233/ajchem.2023.28258
20. V. V. Ghazaryan, M. Fleck, and A. M. Petrosyan, J. Mol. Struc. **977**, 117 (2010). https://doi.org/10.1016/j.molstruc.2010.05.022
21. H. M. Albert and C. L. Gonsago, Growth Aspects of Nonlinear Optical Crystals and Characterization Techniques (Insta Publishing, Chattisgarh, India, 2023).
22. G. S. Kumar,V. Kathiravan, S. Thangavel, K. Thilaga, and P. Selvarajan, J. Mat. Sci. Mat. Electron. **34**, 1531 (2023). https://doi.org/10.1007/s10854-023-10932-7
23. M. Shalini, M. Meena, R. S. Sundararajan, B. S. Ebinezer, T. C. S. Girisun, and E. Manikandan, J. Mat. Sci. Mat. Electron. 34, 1772 (2023). https://doi.org/10.1007/s10854-023-11196-x
24. R. Surekha, S. R. Thilagavathy, P. Sagayaraj, and K. Ambujam, Optik **125**, 934 (2014). https://doi.org/10.1016/j.ijleo.2013.07.109
25. D. Shanthi, P. Selvarajan, and R. J. Mani, Optik **125**, 2531 (2014). https://doi.org/10.1016/j.ijleo.2013.10.118
26. T. U. Devi, N. Lawrence, R. R. Babu, K. Ramamurthi, and G. Bhagavannarayana, J. Min. Mat. Char. Eng. **8**, 755 (2009).
27. G. Ramasamy and S. Meenakshisundaram, Optik **125**, 4422 (2014). https://doi.org/10.1016/j.ijleo.2014.02.036
28. P. Sangeetha, P. Jayaprakash, P. Ramesh, S. Sudha, G. Vinitha, M. Nageshwari, and M. L. Caroline, J. Mol. Struct. **1213**, ID 128187 (2020). doi.org/10.1016/j.molstruc.2020.128187
29. S. Rajyalakshmi, K. R. Rao, B. Brahmaji, K. Samatha, T. V. Rao, and Y. Ramakrishna, J. Mol. Struct. **1129**, 231 (2017). https://doi.org/10.1016/j.molstruc.2016.09.069
30. A. Gupta, R. R. MK, R. O. M. U. Jauhar, V. Sivasubramani, N. Vijayan, G. Vinitha, and L. Nair, Mater. Res. Exp. **6**, 125119 (2020). https://doi.org/10.1088/2053-1591/ab7a5d
31. N. Renuka, R. R. Babu, N. Vijayan, G. Bhagavannarayana, and K.Thukral, Mat. Res. Innov. **20**, 138 (2016). https://doi.org/10.1080/14328917.2016.1149268
32. U. R. Kannan, G. Narayanasamy, S. Subramanian, and P. Selvarajan, IJRAR **5**, 685 (2018).
33. P. K. Devi and K.Venkatachalam, J. Mat. Sci. Mat. Electron **27**, 8590 (2016). https://doi.org/10.1007/s10854-016-4877-7

34. A. Chandramohan, R. Bharathikannan, V. Kandavelu, J. Chandrasekaran, and M. A. Kandhaswamy, Spectrochim. Acta A **71**, 755 (2008). https://doi.org/10.1016/j.saa.2008.01.036
35. K. Ambujam, S. Selvakumar, D. P. Anand, G. Mohamed, and P. Sagayaraj, Cryst. Res. Technol. **41**, 671 (2006). https://doi.org/10.1002/crat.200510647
36. M. L. Caroline, R. Sankar, R. M. Indirani, and S. Vasudevan, Mat. Chem. Phys. **114**, 490 (2009). https://doi.org/10.1016/j.matchemphys.2008.09.070
37. P. Kumaresan, S. M. Babu, and P. M. Anbarasan, Opt. Mat. **30**, 1361 (2008). https://doi.org/10.1016/j.optmat.2007.07.002
38. T. Dhanabal, G. Amirthaganesan, and M. Dhandapani, Optik. **125**, 4341 (2014). https://doi.org/10.1016/j.ijleo.2014.03.027
39. R. A. Jothi, R.U. Mullai, S. Gopinath, E. Vinoth, and S. Vetrivel, Braz. J. Phys. **51**, 1539 (2021). https://doi.org/10.1007/s13538-021-00965-w
40. C. Karnan, A. R. Prabakaran, M. Prabhaharan, and G.Vinitha, J. Electron. Mat. 48, 7915 (2019). https://doi.org/10.1007/s11664-019-07630-8
41. S. K. Chandran, R. Paulraj, and P. Ramasamy, Spectrochim. Acta A **151**, 432 (2015). https://doi.org/10.1016/j.saa.2015.06.113
42. G. C. Bhar, A. K. Chaudhary, and P. Kumbhakar, Appl. Surf. Sci. **161**, 155 (2000). https://doi.org/10.1016/S0169-4332(00)00276-2
43. M. Shalini, R. S. Sundararajan, T. S. Girisun, E. Manikandan, and M. Meena, J. Mat. Sci. Mat. Electron. **33**, 19004 (2022). https://doi.org/10.1007/s10854-022-08733-5
44. P. Karuppasamy, T. Kamalesh, C. S. Kumar, M. S. Pandian, P. Ramasamy, S. Verma, and S. V. Rao, J. Mat. Sci. Mat. Electron. **30**, 1553 (2019). https://doi.org/10.1007/s10854-018-0427-9
45. E. W. V. Stryland and M. Sheik-Bahae, Z-Scan, in Characterization Techniques and Tabulations for Organic Nonlinear Optical Materials, Chapter 8, ed. M. G. Kuzyk et al., (Taylor and Francis Group, New York, 2018) pp. 671-708.
46. A. Steephenraj, C. Sidden, and R. Paulraj, J. Mat. Sci. Mat. Electron. **33**, 22999 (2022). https://doi.org/10.1007/s10854-022-09068-x
47. G. Sudhakar and D. R. Babu, J. Mat. Sci. Mat. Electron. 34, 2153 (2023). https://doi.org/10.1007/s10854-023-11503-6
48. H. M. Albert, P. S. Sagar, J. S. Chandra, N. M. Kumar, J. M. Sailaja, M. K. Chakravarthi et al., J. Nonlin. Opt. Phys. Mat. **24**, 30001 (2024). https://doi.org/10.1142/S0218863524300019
49. B. Lasalle, M. S. Pandian, P. Ramasamy, and K. Anitha, J. Mat. Sci. Mat. Electron. **36**, 1 (2025). https://doi.org/10.1007/s10854-025-14236-w
50. B. S. I. Lasalle, M. S. Pandian, K. Anitha, and P. Ramasamy, J. Mat. Sci. Mat. Electron. **34**, 1527 (2023). https://doi.org/10.1007/s10854-023-10945-2
51. B. S. I. Lasalle, M. S. S. Pandian, K. Anitha, and P. Ramasamy, J. Mat. Sci. Mat. Electron. **34**, 1993 (2023). https://doi.org/10.1007/s10854-023-11354-1
52. B. S. I. Lasalle, M. S. S. Pandian, P. Karuppasamy, V. Sivasubramani, and P. Ramasamy, J. Mat. Sci. Mat. Electron. **35**, 242 (2024). https://doi.org/10.1007/s10854-024-12025-5
53. B. S. I. Lasalle, M. S. S. Pandian, S. Narmadha, P. Karuppasamy, and P. Ramasamy, J. Mat. Sci. Mat. Electron. **36**, 1 (2025). https://doi.org/10.1007/s10854-025-14306-z
54. S. D. Yadav, M. I. Baig, and M. Anis, J. Sci. Res. **17**, 165 (2025). https://orcid.org/0000-0003-1204-9584